AD

TECHNICAL REPORT ARCCB-TR-94046

STRESS CONCENTRATION, STRESS INTENSITY, AND FATIGUE CRACK GROWTH ALONG EVACUATORS OF PRESSURIZED, AUTOFRETTAGED TUBES

A.P. PARKER
J.H. UNDERWOOD

DECEMBER 1994

US ARMY ARMAMENT RESEARCH,
DEVELOPMENT AND ENGINEERING CENTER
CLOSE COMBAT ARMAMENTS CENTER
BENÉT LABORATORIES
WATERVLIET, N.Y. 12189-4050

APPROVED FOR PUBLIC RELEASE; DISTRIBUTION UNLIMITED

DISCLAIMER

The findings in this report are not to be construed as an official Department of the Army position unless so designated by other authorized documents.

The use of trade name(s) and/or manufacturer(s) does not constitute an official indorsement or approval.

DESTRUCTION NOTICE

For classified documents, follow the procedures in DoD 5200.22-M, Industrial Security Manual, Section II-19 or DoD 5200.1-R, Information Security Program Regulation, Chapter IX.

For unclassified, limited documents, destroy by any method that will prevent disclosure of contents or reconstruction of the document.

For unclassified, unlimited documents, destroy when the report is no longer needed. Do not return it to the originator.

REPORT DOCUMENTATION PAGE

Form Approved
OMB No. 0704-0188

1. AGENCY USE ONLY (Leave blank)	2. REPORT DATE	3. REPORT TYPE AND DATES COVERED
	December 1994	Final

4. TITLE AND SUBTITLE
STRESS CONCENTRATION, STRESS INTENSITY, AND FATIGUE CRACK GROWTH ALONG EVACUATORS OF PRESSURIZED, AUTOFRETTAGED TUBES

5. FUNDING NUMBERS
AMCMS: 6111.02.H611.1
PRON: 1A11Z1CANMBJ

6. AUTHOR(S)
A.P. Parker (University of Northumbria at Newcastle, Newcastle, England) and J.H. Underwood

7. PERFORMING ORGANIZATION NAME(S) AND ADDRESS(ES)
U.S. Army ARDEC
Benét Laboratories, AMSTA-AR-CCB-O
Watervliet, NY 12189-4050

8. PERFORMING ORGANIZATION REPORT NUMBER
ARCCB-TR-94046

9. SPONSORING / MONITORING AGENCY NAME(S) AND ADDRESS(ES)
U.S. Army ARDEC
Close Combat Armaments Center
Picatinny Arsenal, NJ 07806-5000

10. SPONSORING / MONITORING AGENCY REPORT NUMBER

11. SUPPLEMENTARY NOTES

12a. DISTRIBUTION / AVAILABILITY STATEMENT
Approved for public release; distribution unlimited

12b. DISTRIBUTION CODE

13. ABSTRACT *(Maximum 200 words)*

A stress analysis has been conducted on a pressurized, fully or partially autofrettaged cylinder with a small diameter evacuator hole penetrating radially through the wall. Pressure was applied on the inside diameter (ID) of the tube, and all or part of this pressure was applied on the evacuator hole surfaces. Total hoop stress concentrations have been determined for a range of radial locations along the evacuator and stress intensity factors have been determined along a crack emanating from the evacuator hole. Fatigue crack growth rates, and hence crack profiles, were predicted at each of the radial locations. These predictions indicate that the critical location for the crack in a non-autofrettaged tube is at the ID, whereas in a fully autofrettaged tube, it is located approximately halfway through the wall thickness. Stress ratio $\sigma_{min}/\sigma_{max}$ has a significant influence on crack shape in autofrettaged tubes, however, it has a limited effect upon lifetime. The effect of axial residual stresses upon fatigue lifetime due to the autofrettage process has been described and an insignificant reduction in lifetime was a result of such stresses. Finally, the predicted profiles are compared with experimental observations of fatigue crack evacuators, and a limited comparison of predicted and actual lifetimes is presented. Good agreement has been observed in both comparisons.

14. SUBJECT TERMS
Crack Growth, Fatigue Cracks, Cylinders, Evacuators, Cross-Bore, Fracture (Materials), Fracture Mechanics, Residual Stress, Stress Intensity Factor, Stress Ratio

15. NUMBER OF PAGES
24

16. PRICE CODE

17. SECURITY CLASSIFICATION OF REPORT	18. SECURITY CLASSIFICATION OF THIS PAGE	19. SECURITY CLASSIFICATION OF ABSTRACT	20. LIMITATION OF ABSTRACT
UNCLASSIFIED	UNCLASSIFIED	UNCLASSIFIED	UL

TABLE OF CONTENTS

Tables

List of Illustrations

ACKNOWLEDGEMENTS

The authors are pleased to acknowledge the help of D.J. Corrigan, R.A. Farrara, and M.J. Audino of Benét Laboratories in the collection and interpretation of the experimental results described here. The first author, A.P. Parker, performed work on this report as a visiting scientist at Benét Laboratories.

NOMENCLATURE

a	Crack depth
f	Final
C	Coefficient in Paris' crack growth law
d	Diameter of evacuator hole
eff	Effective
i	Initial
ID	Inside diameter
K	Stress intensity factor
k_t	Stress concentration factor
ln	Natural logarithm
OD	Outside diameter
m	Exponent in Paris' crack growth law
max	Maximum value
min	Minimum value
N	Number of fatigue cycles
p	Pressure
p*	Autofrettage pressure
r	Radial coordinate
R	Stress ratio $\sigma_{min}\sigma/_{max}$
R_1	Tube inner radius
R_2	Tube outer radius
R_A	Maximum radius of yielding in autofrettage process
Y	Yield stress

z	Axial coordinate
α	Ratio of biaxial stresses
σ	Direct stress
σ^*	Maximum stress at stress concentrator
θ	Angular coordinate
$\Delta\sigma$	Stress range
ΔK	Stress intensity factor range

INTRODUCTION

The phenomenon of stress concentration, stress intensity, and fatigue crack growth in pressurized thick-walled cylinders is well-known and relatively well-understood. To date, the features of such geometries that have been addressed in detail include:

- Single and multiple internal and external radial cracks, straight-fronted, and semi-elliptical
- Full or partial autofrettage of the tube
- External notch effects
- Internal notch effects

In general, the above analyses all encompassed two-dimensional geometries prior to the introduction of the cracks. In this report, the study is extended to encompass an associated geometry which is truly three-dimensional prior to the introduction of the crack.

THE PRESENCE OF AN EVACUATOR HOLE

The purpose of this report is to extend the analysis of the basic pressurized thick-walled cylinder, internal radius R_1, external radius R_2, and internal pressure p, see Figure 1. Note that the internal pressure is maintained by a piston, implying zero net longitudinal force, and hence negligible longitudinal stress in the tube. The modification, which is the subject of this analysis, is illustrated in Figure 2, and consists of a single radial vent (or evacuator) of diameter $d(d << 2R_1)$ that pierces the tube radially at a 90-degree angle to the longitudinal axis. Such evacuators are sometimes angled at less than 90 degrees--a typical value is 30 degrees (ref 1). This effect is considered later in this report.

STRESSES IN THE ORIGINAL TUBE

The tube prior to the introduction of the radial vent is illustrated in Figure 1. The hoop stresses () in this geometry arise from two sources, namely internal pressure and autofrettage. The hoop stresses due to internal pressure p are given by the familiar Lamé equations, (ref 2):

$$\sigma_{\theta Lamé} = \left(\frac{pR_1^2}{R_2^2 - R_1^2}\right)\left(1 + \frac{R_2^2}{r^2}\right) \qquad (1)$$

while the stresses due to autofrettage (ref 3) are

$$\sigma_{\theta autofrettage} = -p* + Y(1+\ln(r/R_1)) - p*\left(\frac{R_1^2}{R_2^2-R_1^2}\right)\left(1+\frac{R_2^2}{r^2}\right) \qquad R_1 \le r \le R_A \tag{2}$$

$$\sigma_{\theta autofrettage} = \left(\frac{YR_A^2}{2R_2^2} - \left(\frac{p*R_1^2}{R_2^2-R_1^2}\right)\right)\left(1+\frac{R_2^2}{r^2}\right) \qquad R_A \le r \le R_2 \tag{3}$$

where p*, the autofrettage pressure, is given by:

$$p* = Y\ln(R_A/R_1) + Y\left(\frac{R_2^2-R_A^2}{2R_2^2}\right) \tag{4}$$

where Y is the yield strength of the material and R_A is the maximum radial extent of the elastic/plastic boundary during the autofrettage process.

The axial direct stress, σ_z, resulting from the application of internal pressure p is zero in cases where a piston contains the pressure in the bore and is much less than the hoop stress even when the ends are sealed. Since the objective is to determine stress concentration and stress intensity factors at critical locations, we focus solely upon critical locations and planes. This analysis could be easily extended to determine von Mises' stresses if so desired.

For purposes of the initial analysis, axial residual stresses are assumed to be zero. This conforms with normal practice. However, it is known that axial stresses may be present in autofrettaged tubes, and it is likely that different methods of manufacture, whether hydraulic or swage, may produce significant differences. While the contribution of axial stress to stress intensity of cracks in the r plane is zero in the absence of stress concentrators, this is not the case for cracks emanating from a stress concentrator. Furthermore, on r planes the concentrator reverses the sign of any axial residual stress. This effect is discussed further in another section of this report.

STRESSES IN THE VICINITY OF THE EVACUATOR

Pressure is released from the bore into the evacuator by the movement of the piston, and the determination of pressure within the hole requires a complex analysis (ref 4). Somewhat surprisingly, pressure in the hole in this case is reasonably constant throughout its length and is approximately 20 percent of the bore pressure.

Stresses contributing to the maximum stress concentration in the vicinity of the evacuator may arise from three sources and can be summarized as:

$$\sigma_{total} = k_1\sigma_{Lamé} + k_t\sigma_{autofrettage} + \sigma_{pressure}$$

where the various components are listed below:

$k_t\sigma_{Lamé}$ is the concentration of the Lamé stresses given by Eq. (1). Since $d << 2R_1$, the stress concentration effect, k_t is for an infinite plate in uniaxial tension, namely a factor of 3.0 for a circular hole.

$k_t\sigma_{autofrettage}$ is the concentration of the autofrettage stresses presented in Eqs. (2), (3), and (4). This factor is 3.0.

$\sigma_{pressure}$ are the hoop stresses arising from internal pressure within the evacuator hole. Using the Lamé stresses for $d << 2R_1$, the tensile hoop stress has the same magnitude as the evacuator hole pressure.

The variation of the maximum hoop stresses along the evacuator in a cylinder of diameter ratio 1.5 with an evacuator normal to the tube axis is presented in Figure 3. For this illustration, R_1 = 60 mm, R_2 = 90 mm, evacuator diameter, d = 4 mm, and the pressure acting on the tube inside diameter (ID) is 150 MPa with 20 percent of this value (30 MPa) acting on the evacuator hole surface. For the autofrettage stress calculations, the yield strength is assumed to be 1200 MPa. There is a relatively insignificant contribution arising from pressure in the evacuator hole; generally the contribution from pressure in the evacuator amounts to less than 10 percent of the stress range, while extremely high stress levels result from concentration of the Lamé and autofrettage stresses. These high values are encountered at the ID of the non-autofrettaged tube and at the outside diameter (OD) in the case of 100 percent autofrettage. By comparison, Figure 3 also shows the effect of 25 and 50 percent autofrettage. The elimination of the extreme peaks of stress near the ID and OD as a result of 25 or 50 percent autofrettage is clear. In this example no attempt is made to limit stress values at the yield value so that we can retrospectively examine the potential effects of such a limitation.

STRESS RANGE AND STRESS RATIO EFFECTS

The stress range during the loading cycle, $\Delta\sigma$, is given by

$$\Delta\sigma = \sigma_{max} - \sigma_{min} \qquad \sigma_{min} > 0 \tag{5}$$

$$\Delta\sigma = \sigma_{max} \qquad \sigma_{min} < 0 \tag{6}$$

(Note: min may be less than zero at the tube radii which contain compressive residual stress arising from full or partial autofrettage.)

The stress ratio, R, is given by

$$R = \sigma_{min}/\sigma_{max} \qquad \sigma_{min} > 0 \tag{7}$$

$$R = 0 \qquad \sigma_{min} < 0 \tag{8}$$

The importance of a clear understanding of stress range and stress ratio in the presence of residual stresses is discussed in Reference 6. The variation of stress ratio and stress range is illustrated in Figure 4 for cases 0, 25, 50, and 100 percent autofrettage. This clearly illustrates the relatively constant stress range near the OD, regardless of the amount of autofrettage, with the significant variations in stress ratio reaching values of approximately 0.63.

STRESS INTENSITY ESTIMATES

The dominant loading and geometry for the configuration under consideration is a circular hole with two diametrically opposed equal length radial cracks in a large plate loaded remotely in uniaxial tension, i.e., $\alpha = 0$, Figure 5a. This is an appropriate representation for the hoop loading resulting from residual stress and from internal pressure on the cylinder bore. In the evacuator hole, this is loaded internally by approximately 20 percent of the bore pressure, and it may be assumed that this pressure acts on both the hole surface and the crack faces, Figure 5b. Since the stress intensity factor for an internally pressurized, cracked geometry is identical to the stress intensity for a remote biaxial tension of equal magnitude to that of the internal pressure, we may address the calculation of all contributions to stress intensity by appropriate superposition of stresses α and $\alpha\sigma$.

Accurate stress intensity factors for this geometry have been calculated by Bowie and Newman (ref 7). The limiting value at short crack lengths is given by

$$K_1 = 1.12\sigma * \sqrt{\pi\alpha} \tag{9}$$

where * is equal and opposite to the direct stress at the origin of the prospective crack. The above approximation was compared with solutions at longer crack lengths. In the case considered here, the bulk of the fatigue lifetime is expended at very short crack lengths, and the use of the limiting value does not produce errors in lifetime calculations greater than 10 percent. Furthermore, the assumption is a conservative one.

INTEGRATION OF CRACK GROWTH LAW

The well-known Paris law relating crack growth per loading cycle (da/dN) to stress intensity range (ΔK) is given by (ref 8)

$$\frac{da}{dn} = C(\Delta K)^m \tag{10}$$

where C and m are experimentally-determined material 'constants'. (Note that dimensional homogeneity is achieved through the dimensions of C.)

In this case it was necessary to solve Eq. (10) precisely on the basis of Eq. (9) for the number of cycles, N, required for the crack to propagate from a crack length a_i to a length a_f. To achieve this, Eq. (10) was integrated and rearranged to give:

$$\int_{a_i}^{a_f} = \frac{da}{C(\Delta K)^m} = N \tag{11}$$

and hence, substituting

$$\Delta K = 1.12\Delta\sigma\sqrt{\pi a} \tag{12}$$

together with the Paris law exponent m = 3 yields on integration

$$a_f = \left[\frac{2}{2/\sqrt{a_i} - NC(1.12\sigma\sqrt{\pi})^3}\right]^2 \tag{13}$$

which will be useful in predicting final crack-depth profiles for comparison with experimental observation.

CRACK PROFILE PREDICTIONS

Values of stress range may be used, via Eq. (12), to determine accurate values of stress intensity range at very short crack lengths, while at longer crack lengths, the results presented in Reference 7 may be used if necessary. The stress intensity range may, in turn, be employed, via suitable experimental data on crack growth per loading cycle (da/dN) in the determination of crack growth arising from 1000 cycles of loading. Such data for the steel under consideration was obtained from Reference 5, specifically $C = 6.52 \times 10^{-12}$ and m = 3 for ΔK in MPA√m and crack growth in m per cycle. Reference 9 provides some data on R ratio effects, however, initially it was assumed that R ratio is fixed at zero, and fatigue crack growth predictions were constructed on this basis.

In order to predict a crack growth profile, it was assumed that two pre-existing straight-fronted, diametrically-opposed cracks 0.01-mm deep were present along the evacuator bore prior

to cyclic loading. This assumption was considered reasonable since there was pre-existing cracking arising from heat checking over a considerable length of the evacuator bore.

The stress intensity range, and hence the fatigue crack growth resulting from given numbers of fatigue cycles, was evaluated at the ID, the OD, and at five intermediate points on the crack front. Each of the new crack lengths was then employed in a new stress intensity and crack growth rate calculation, and so on. The resulting crack profile predictions using Eq. (13) are presented in Figure 6. In each case the crack was allowed to propagate until the maximum value of stress intensity on the crack front reached a critical value of approximately 100 MPa$\sqrt{m}$. Since lifetime is extremely insensitive to the choice of final crack length, this value of stress intensity likewise had little effect on total lifetime.

These results indicate clearly that:

1. The magnitude of the fatigue crack growth for a given number of cycles is highest in the non-autofrettaged tube.

2. The maximum crack depth occurs at the bore in the non-autofrettaged tube.

3. The maximum crack depth in the autofrettaged tubes is well removed from the bore.

R RATIO EFFECTS

Thus far R ratio has been considered constant. The effects of R ratio can be significant (ref 6) and should be taken into account. For example, in this investigation, at a fixed K, the crack growth rate for an R ratio of 0.5 is some 20 percent higher than for an R ratio of zero (ref 9). Referring back to Figure 4, it is observed that R ratio varies from 0 to 0.63. Introducing this effect on the basis of data in Reference 9, the crack profile results are modified as shown in Figure 7. The effects are significant in the autofrettaged tubes, particularly in the case of 100 percent autofrettage. In all cases there is an increase in predicted crack depth at the OD, and in the case of 100 percent autofrettage, the crack is predicted to be significantly deeper between the midpoint and the OD for much of the component lifetime. This effect is compared further in Figure 8, which directly compares profiles for the case of 100 percent overstrain at a fixed number of cycles for the case in which R ratio is considered and ignored. While R ratio produces a significant effect in terms of crack profile, it reduces lifetime by only 18 percent for 100 percent overstrain and by lesser amounts for reduced overstrain.

In retrospect, it is possible to see that even in the 100 percent autofrettaged tube, the critical location is somewhat removed from the OD. Hence, even if the concentrated residual stresses had been limited, this would not have affected the above predictions.

COMPARISON WITH EXPERIMENTAL RESULTS

Davidson, Brown, and Kendall (ref 1) have described laboratory fatigue tests of thick-walled cylinders with evacuator holes of the type used with cannon. They found considerable decreases in fatigue life due to holes, and they reported further decreases in life for a hole at 30 degrees to the cylinder axis compared with a radial hole (at 90 degrees). Chaaban and Barake (ref 10) reported elastic and elastic-plastic stresses near radial holes in pressurized cylinders, with a hole diameter-to-cylinder diameter ratio of 0.2. Their results do not vary significantly from the limiting $k_t = 3$ result for a hole in a wide plate.

Comparison is made here with recent unpublished Army results of fatigue tests of cylinders with a 3.6-mm diameter hole at 30 degrees to the cylinder axis, a configuration commonly used in a cannon to evacuate gasses after firing. Table 1 lists some test conditions and a comparison of measured and calculated fatigue life results. Figure 9 shows macrophotographs of fracture surfaces from test samples broken open after the fatigue tests were completed. Note that the crack growth for tube #1A, which was not autofrettaged, is highly concentrated near the ID surface, as was predicted by analysis as shown in Figures 6a and 7a. For the autofrettaged tube #2, the crack growth profile was generally similar to that shown in Figures 7c and 7d for the 50 and 100 percent autofrettage cases. Therefore, general agreement exists between the analytically predicted crack growth profiles and those observed from the tests.

Quantitative comparisons were made between calculated and measured fatigue lives, as summarized in Table 1. As seen in Figure 9, the measured fatigue lives do not quite correspond to the final growth of the crack through to the OD. The test was stopped when leaks occurred at the threads seen in the photographs. Nevertheless, since fatigue life is very insensitive to the final portion of crack growth, the measured lives are expected to be very nearly correct. The calculated lives were determined from Eq. (13) in different form, in a manner similar to that of prior work (ref 11)

$$N = 2\left[1/\sqrt{a_i} - 1/\sqrt{a_f}\right]/C\left[1.12h\sigma_{eff}\sqrt{\pi}\right]^3 \tag{14}$$

where the total effective stress, σ_{eff}, is made up of three parts

$$\sigma_{eff} = k_t\sigma_{autofrettage} + k_t\sigma_{Lamé} + 2p \tag{15}$$

and

$$k_t\sigma_{autofrettage} \le \sigma_{yield} \tag{16}$$

The first term, $k_t\sigma_{autofrettage}$, accounts for the autofrettage residual stresses as concentrated by the hole (note the limit that has been applied); the second term, $k_t\sigma_{Lamé}$, accounts for the concentrated cylinder Lamé stresses; the third term, 2p, accounts for the evacuator hole Lamé stress at the hole ID (p for a small hole) and for the pressure in the crack (also = p (ref 11)). Life calculations were made using the following inputs to Eqs. (14) and (15): $a_i = 0.01$ mm; $a_f =$ (OD-ID)/2; C as described previously; $h = 0.64$ to account for the semi-elliptical crack shape (seen in Figure 8); $k_t = 3$ for the hole; $Y = 1200$ MPa. Autofrettage and Lamé values were calculated from Eqs. (1) and (2) at the location along the hole with the highest stress range. It is

important to note that this location is the cylinder ID for the non-autofrettaged tube and about midwall for the autofrettaged tube, as shown in Figure 4. Both the predicted crack profiles of Figures 6 and 7 and the experimental behavior seen in Figure 9 are consistent with these locations of highest stress range.

Referring again to the comparison of measured and calculated lives in Table 1, the agreement is good, considering the many factors that can affect fatigue tests. This agreement, combined with the good comparison between predicted and measured crack size profiles discussed previously, indicate that the methods of analysis described here are useful for pressure vessel fatigue life design and analysis. More detailed comparisons of fatigue life calculations and test results are the subject of continuing work by the authors.

Table 1. Specimen Configuration and Test Conditions

Tube Number	Tube Size at Evacuator		Amount of Autofrettage	Measured Life	Calculated Life
	R_1 (mm)	R_2 (mm)			
1A	53	76	None	4,710	4,300
1B	53	76	None	5,770	4,300
2	53	81	100%	9,780	12,200

EFFECTS OF NON-ZERO AXIAL RESIDUAL STRESS

Thus far it has been assumed that axial direct stress, σ_z, is zero. Accurate determination of axial residual stress arising from the autofrettage process is complex. However, in the case of an ideal elastic-perfectly plastic process, it may be represented with reasonable accuracy by (ref 3)

$$\sigma_{z_{autofrettage}} = \nu\left(\sigma_{\theta_{autofrettage}} + \sigma_{r_{autofrettage}}\right) \tag{17}$$

The residual stresses for 100 percent overstrain are given by (ref 3)

$$\sigma_{\theta_{autofrettage}} = Y\left[1 + \ln(r/R_2) - (R_1^2/(R_2^2 - R_1^2))(1 + R_2^2/r^2)(\ln(R_2/R_1))\right] \tag{18}$$

$$\sigma_{r_{autofrettage}} = Y\left[\ln(r/R_2) - (R_1^2/(R_2^2 - R_1^2))(1 - R_2^2/r^2)(\ln(R_2/R_1))\right] \tag{19}$$

Hence, substituting from Eqs. (18) and (19) into Eq. (17)

$$\sigma_{z_{autofrettage}} = \nu\left[1 - (2R_1^2/(R_2^2 - R_1^2))(\ln R_2/R_1) + 2\ln(r/R_2)\right] \tag{20}$$

Thus far it has been observed that the critical radial location, i.e., the point at which fatigue crack growth is a maximum, is at that point on the evacuator hole boundary at which the residual stress field becomes positive. This is because it represents the point at which the stress range reaches a maximum value, as shown in Figure 4. Note that the residual stress field of interest is due to the concentration of the autofrettage hoop stress, i.e., where $k_t\sigma_{\theta autofrettage} = 3$ for a small diameter hole at the point at 90 degrees to the direction of loading. However, the concentration of axial residual stress on the plane of interest arises as a result of the concentration effect at 0 degrees to the direction of loading, a factor of -1 for any elliptical cutout (ref 2). Thus the total contribution to residual hoop stress at the evacuator is given by

$$\sigma_{\theta_{total}} k_t\sigma_{\theta_{autofrettage}} - \nu\left(\sigma_{\theta_{autofrettage}} + \sigma_{r_{autofrettage}}\right) \tag{21}$$

or

$$\sigma_{\theta_{total}} = (k_t - \nu)\sigma_{\theta_{autofrettage}} - \nu\sigma_{r_{autofrettage}} \tag{22}$$

Hence the point at which the concentrated residual stress acting along the evacuator becomes positive is altered by the contribution from the term $-\nu\sigma_{rautofrettage}$. The determination of the value of r at the point at which the concentrated residual stress field changes sign requires a simple iterative solution using Eqs. (18) through (22). Table 2 shows the radius r at which the sign change occurs for $R_2/R_1 = 1.5$ and 2.0. This is presented for the case of z zero and of z non zero. In the latter case, the axial stress is given by Eq. (17).

Table 2. Effect Upon Fatigue Crack Growth Rate of Presence of Axial Residual Stress

R_2/R_1	$\sigma_z = 0$		σ_z From Eq. (17)		$\Delta\sigma_2/\Delta\sigma_1$	Change in da/dN
	r/R_1	$\Delta\sigma_1/k_t\,p$	r/R_1	$\Delta\sigma_2/k_t\,p$		
1.5	1.234	1.9821	1.2305	1.9889	1.0034	+1.0%
2.0	1.445	0.9719	1.435	0.9808	1.0092	+2.8%

Knowing r, it is possible to determine the stress range $\Delta\sigma$ due to the concentrated Lamé hoop stresses at this point. The ratio of the stress ranges is presented in column 6. Small differences in stress range are apparent. However, in order to predict the impact upon fatigue crack growth rate, it is necessary to raise this ratio to the power m (the Paris law exponent). In this case, m = 3, and the resultant increase in crack growth rate is shown in column 7. The effects are very small, with a maximum increase in crack growth rate of 1.0 and 2.8 percent for $R_2/R_1 = 1.5$ and 2.0, respectively.

DISCUSSION AND CONCLUSIONS

Life predictions for cracked tubes require an accurate knowledge of stress intensity factors at short crack lengths. In this report, stress intensity solutions for pressurized, autofrettaged and partially autofrettaged tubes with cracks emanating from small diameter radial evacuator holes are calculated. These solutions are presented for a variety of locations along the evacuator and are used to predict crack profiles arising from fatigue loading of the tube. In this fatigue loading, pressure acts on the bore of the tube, within the evacuator hole, and on the crack surfaces. These profile predictions indicate:

1. The magnitude of the fatigue crack growth for a given number of cycles is highest in the non-autofrettaged tube.

2. The maximum crack depth in the non-autofrettaged tube occurs at the bore.

3. The maximum crack depth in the autofrettaged tubes is well removed from the bore.

4. Introduction of stress ratio effects produces a significant change in the predicted crack profile in autofrettaged tubes, extending the maximum crack depth towards the tube's outside diameter. However, there is a limited effect upon lifetime.

In comparisons with experimental data, the significant features of crack profiles matched the earlier predictions, and fatigue lifetimes calculated on the basis of a stress intensity that varies along the evacuator likewise provided good agreement.

An accurate procedure for estimating the impact upon fatigue lifetime of the presence of axial residual stresses indicates that for the tube geometry in this case, such stresses reduce fatigue lifetime by 1 percent.

While autofrettage is beneficial in extending lifetime, the factor by which lifetime is improved is not as great as in tubes without evacuators. This is because the very large stress concentration effects tend to produce cycling at levels close to the yield strength of the material, thereby eliminating some of the advantageous residual stress.

REFERENCES

1. T.E. Davidson, B.B. Brown, and D.P. Kendall, *Materials and Processes Considerations in the Design of Pressure Vessels,* 2nd International Conference on High Pressure Technology, Brighton, I Mech E, 1977, pp. 63-71.

2. S.P. Timoshenko and J.M. Goodier, *Theory of Elasticity*, 3rd Edition, McGraw Hill, 1970.

3. R. Hill, *The Mathematical Theory of Plasticity,* Oxford University Press, 1967.

4. H.T. Nagamatsu, K.Y. Choi, R.E. Duffy, and G.C. Carofano, "An Experimental and Numerical Study of the Flow Through a Vent Hole in a Perforated Muzzle Brake," U.S. Army ARDEC Technical Report ARCCB-TR-87016, Benét Laboratories, Watervliet, NY, June 1987.

5. A.P. Parker, J.H. Underwood, J.F. Throop, and C.P. Andrasic, " Stress Intensity and Fatigue Crack Growth in a Pressurized, Autofrettaged Thick Cylinder," *Fracture Mechanics: Fourteenth Symposium - Volume 1: Theory and Analysis, ASTM STP 791,* 1983, pp. 1-216-1-237.

6. A.P. Parker, "Stress Intensity Factors, Crack Profiles, and Fatigue Crack Growth Rates in Residual Stress Fields," *Residual Stress Effects in Fatigue, ASTM STP 776,* 1982, pp. 13-31.

7. D.P. Rooke and D.J. Cartwright, *Compendium of Stress Intensity Factors,* HMSO, London, 1976.

8. P.C. Paris and F. Erdogan, *Journal of Basic Engineering, Trans ASME,* Vol. 85, 1963, pp. 528-534.

9. *Damage Tolerant Design Handbook,* Metals and Ceramics Information Center, Battelle Columbus Laboratories, December 1983.

10. A. Chaaban and N. Barake, "Elasto-Plastic Analysis of High Pressure Vessels with Radial Cross-Bores," *High Pressure - Codes, Analysis, and Applications, PVP Vol. 263*, American Society of Mechanical Engineers, New York, 1993, pp 67-71.

11. J.H. Underwood and A.P. Parker, "Fatigue Life Analysis and Tests for Thick-Walled Cylinders Including Effects of Overstrain and Axial Grooves," U.S. Army ARDEC Technical Report ARCCB-TR-94038, Benét Laboratories, Watervliet, NY, September 1994.

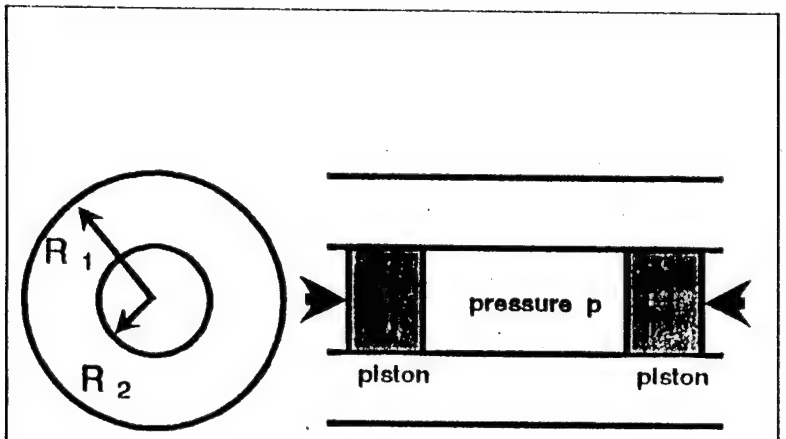

Figure 1 : Pressurized Tube - Geometry and Loading

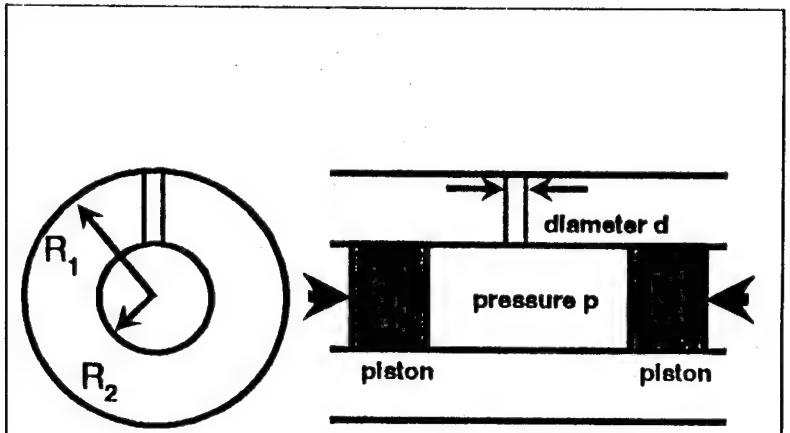

Figure 2 : Pressurized Tube with Evacuator

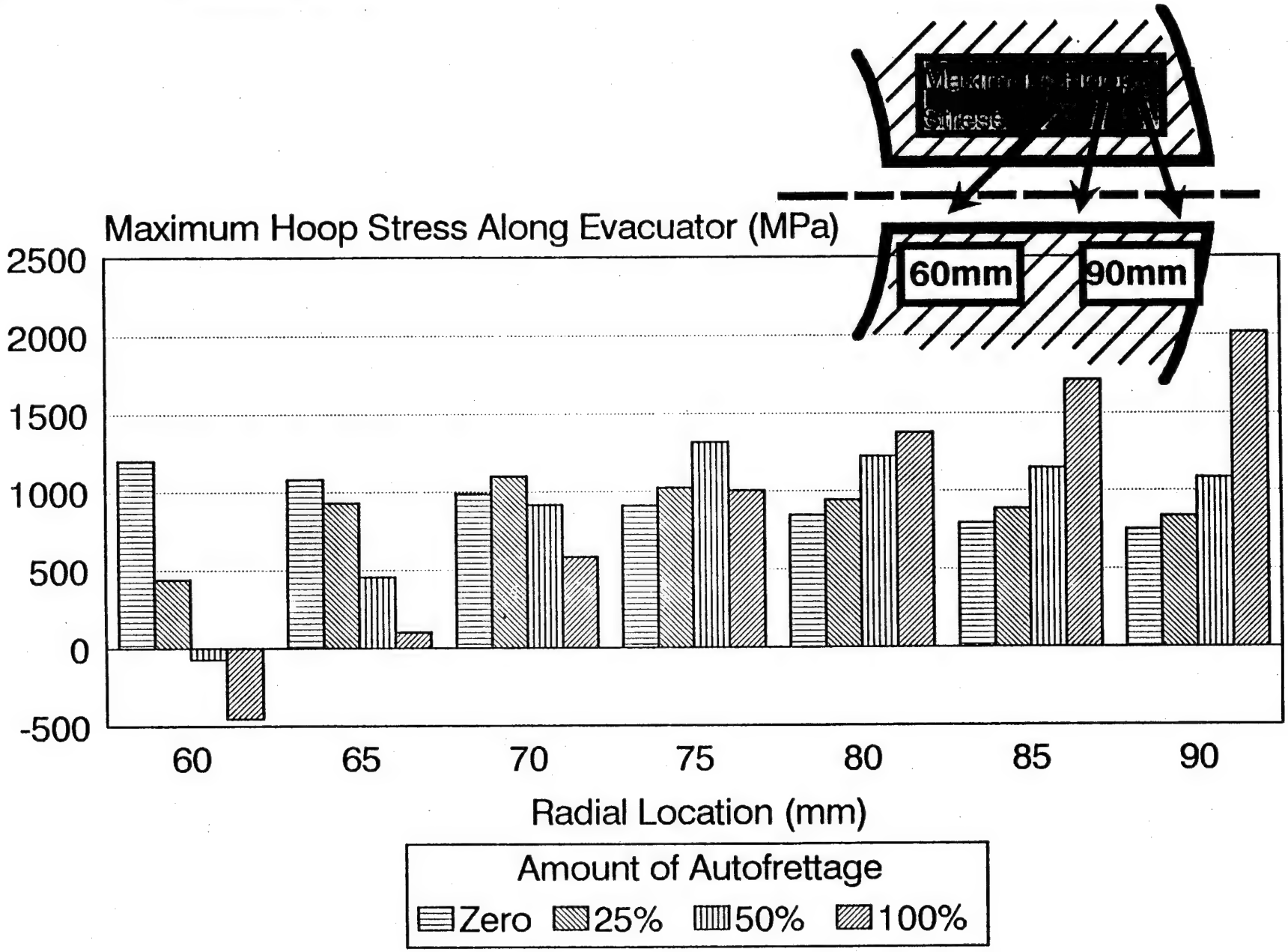

Figure 3: Variation of Maximum Hoop Stress at Various Axial Locations Along Evacuator in Pressurized, Non-Autofrettaged, Partially-Autofrettaged, and Fully-Autofrettaged Tubes.

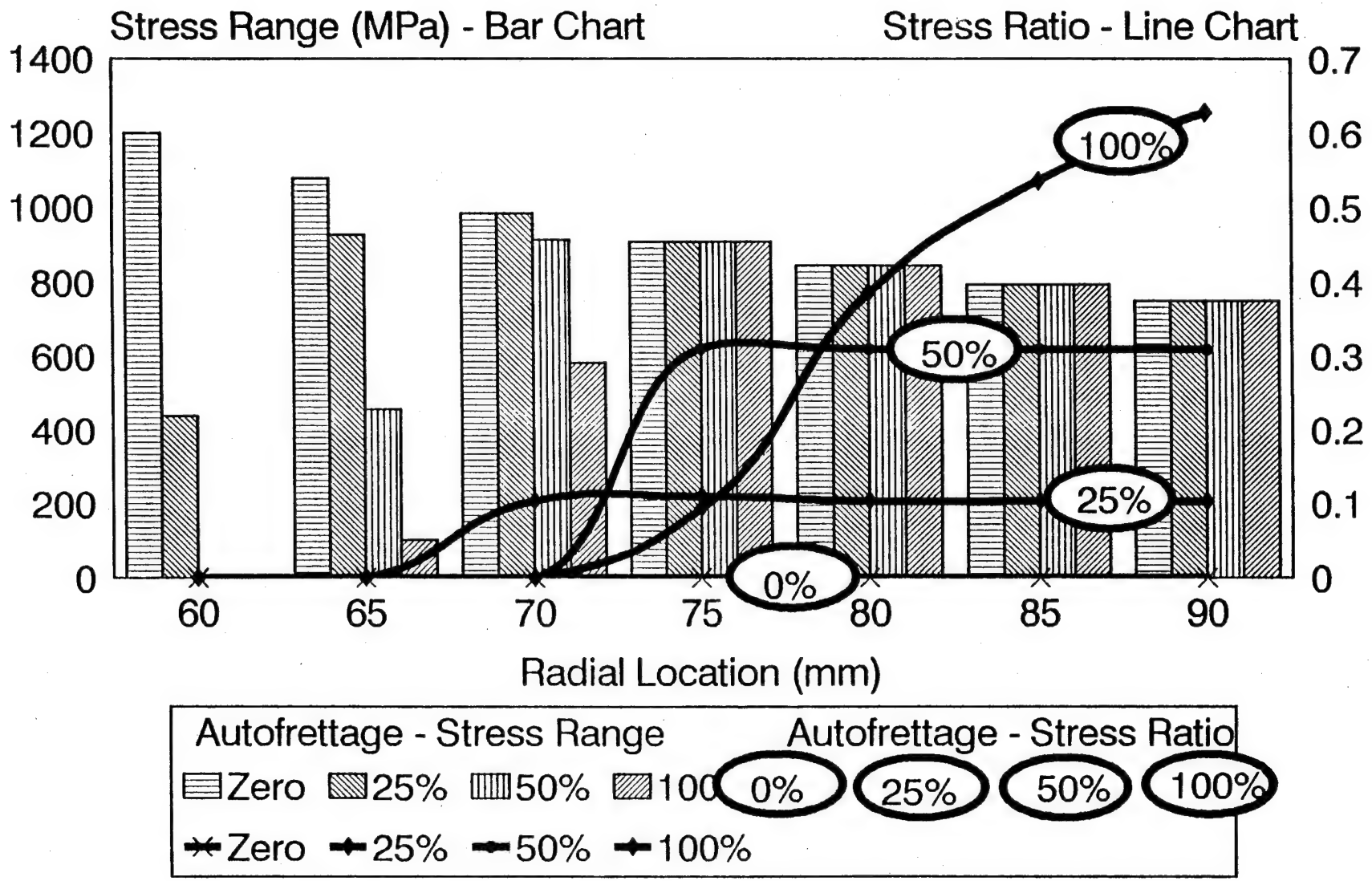

Figure 4: Variation of Stress Range, $\Delta\sigma$, and Stress Ratio, R, at Different Axial Locations Along the Evacuator.

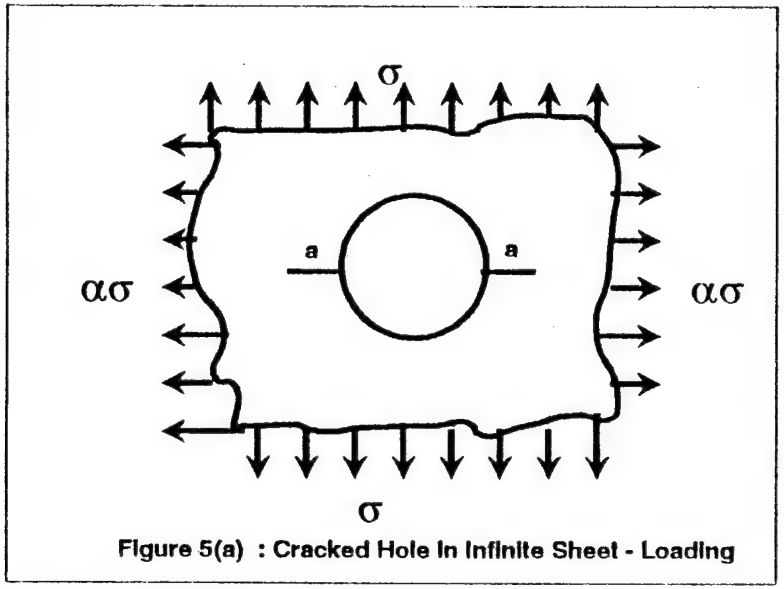

Figure 5(a) : Cracked Hole In Infinite Sheet - Loading

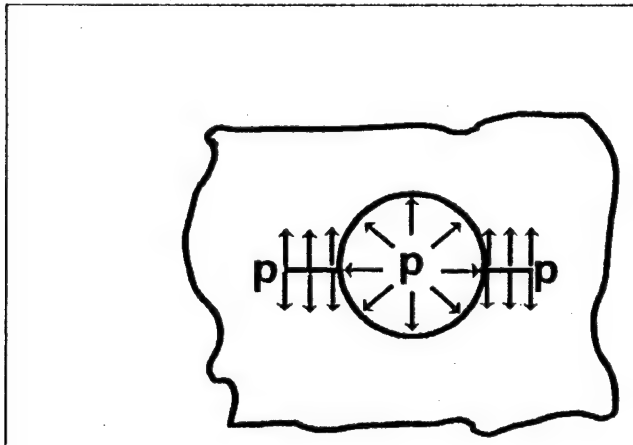

Figure 5(b) : Cracked Hole In Infinite Sheet - Pressure

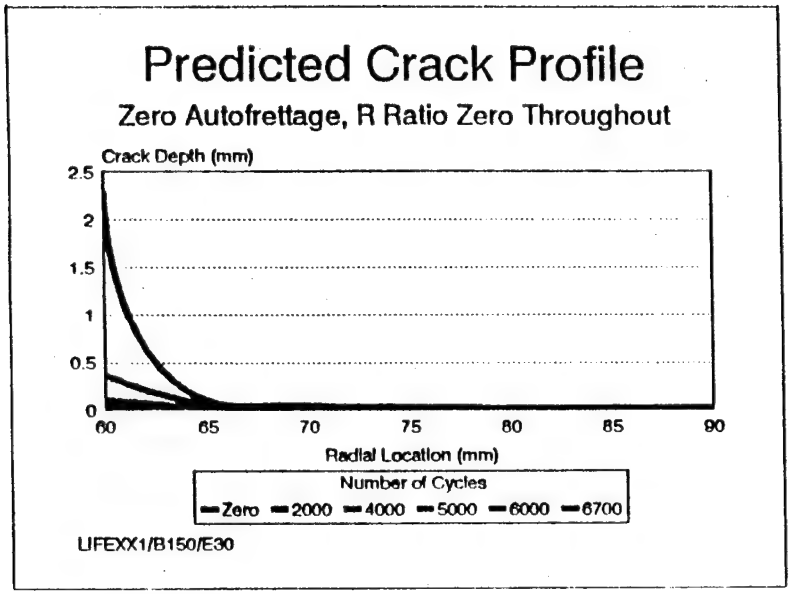

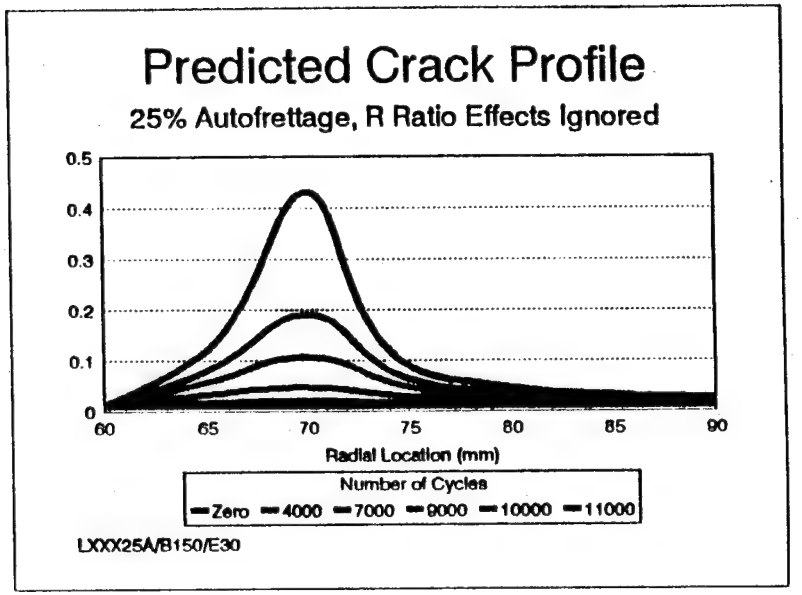

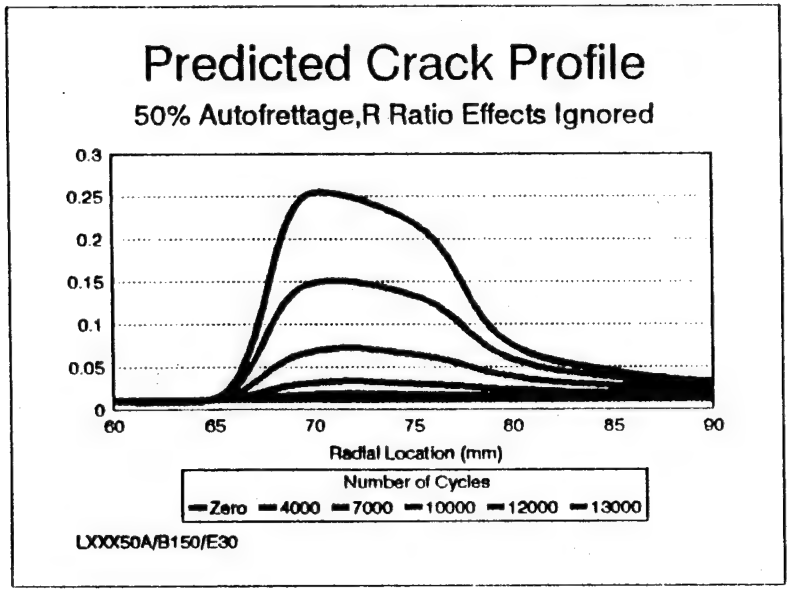

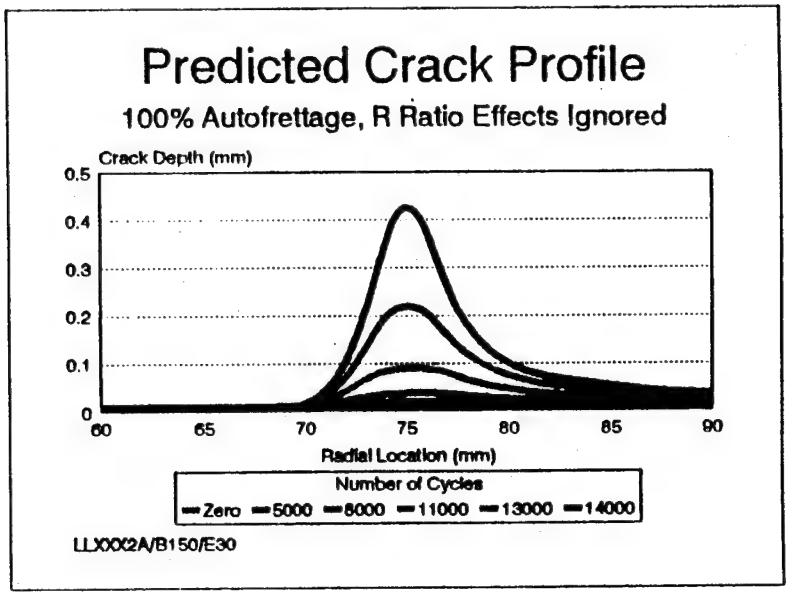

Figure 6: Predicted Crack Profiles Along Evacuator Bore in Non-Autofrettaged, Partially-Autofrettaged and Fully-Autofrettaged Tubes Excluding R Ratio Effects.

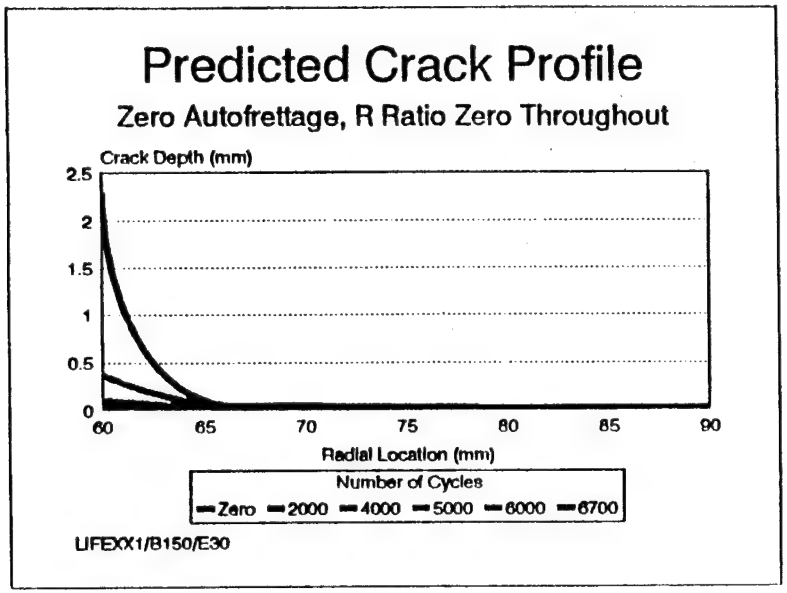

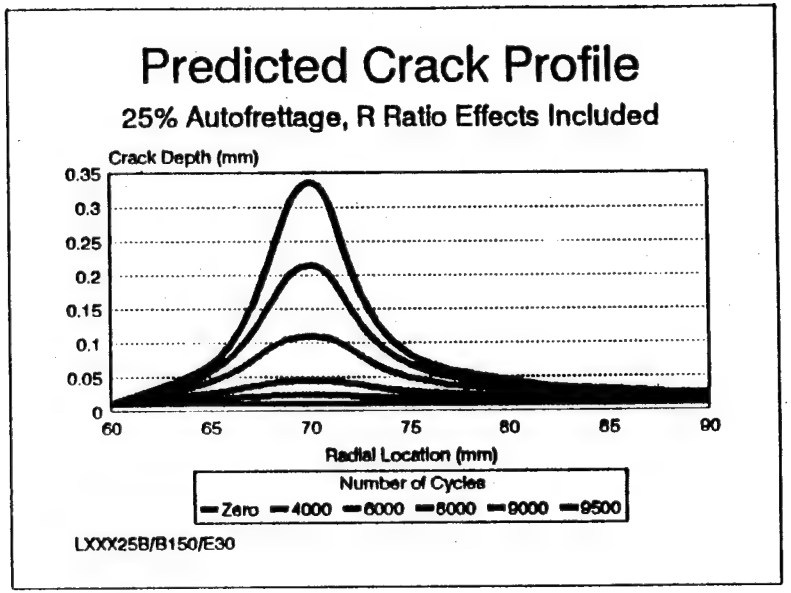

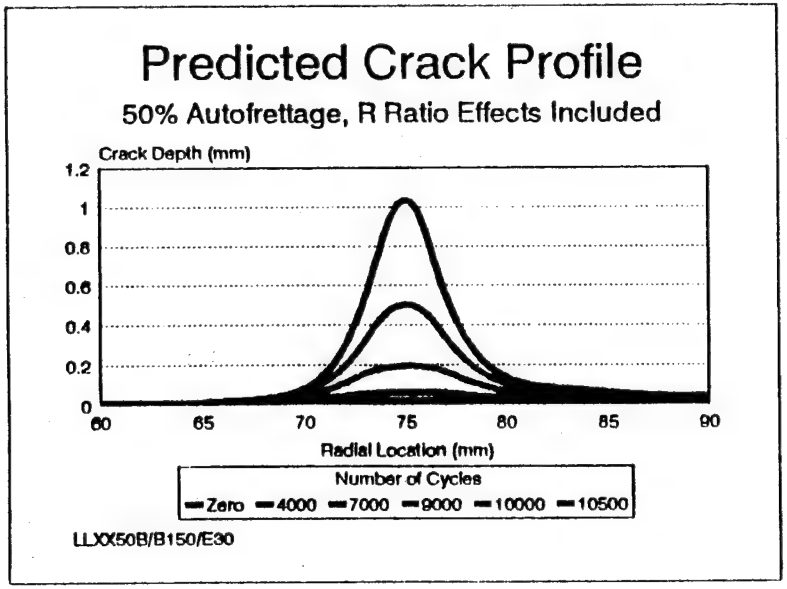

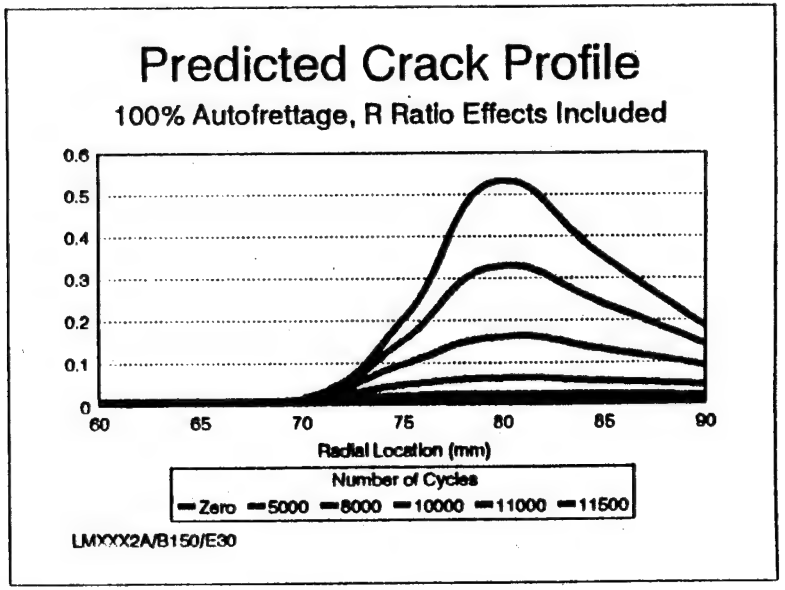

Figure 7: Predicted Crack Profiles Along Evacuator Bore in Non-Autofrettaged, Partially-Autofrettaged and Fully-Autofrettaged Tubes Incorporating R Ratio Effects.

Predicted Crack Profile

100% Autofrettage, with and without R Ratio Correction

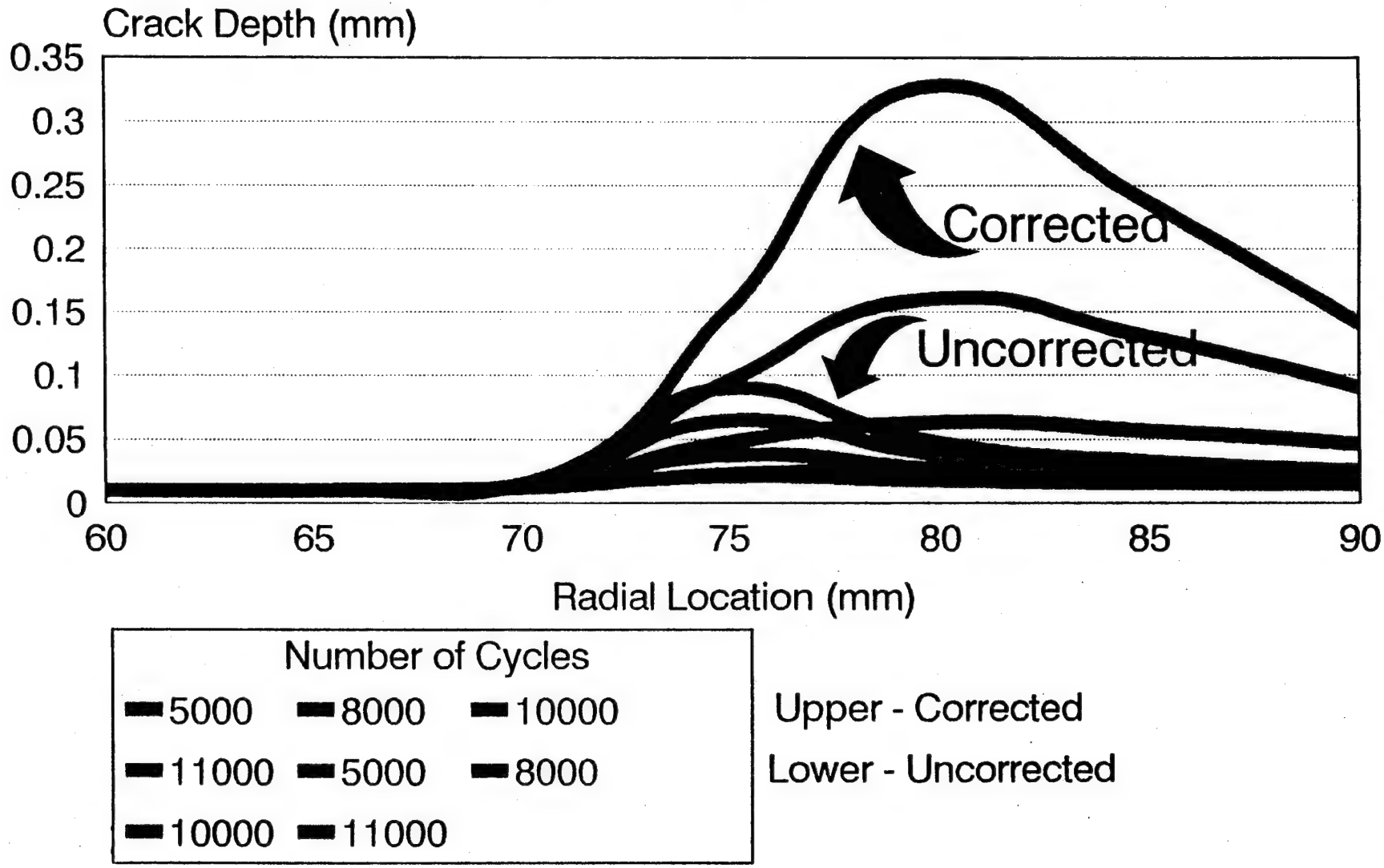

Figure 8: Predicted Crack Profiles Along Evacuator Bore in a 100% Autofrettaged Tube
Direct Comparison of Effects of Including and Not Excluding R Ratio.

Tube #1A, No Autofrettage.

Tube #2, 100% Autofrettage.

Figure 9: Fracture Surfaces From Fatigue Tests (1.4X).

TECHNICAL REPORT INTERNAL DISTRIBUTION LIST

	NO. OF COPIES
CHIEF, DEVELOPMENT ENGINEERING DIVISION	
ATTN: AMSTA-AR-CCB-DA	1
-DB	1
-DC	1
-DD	1
-DE	1
CHIEF, ENGINEERING DIVISION	
ATTN: AMSTA-AR-CCB-E	1
-EA	1
-EB	1
-EC	
CHIEF, TECHNOLOGY DIVISION	
ATTN: AMSTA-AR-CCB-T	2
-TA	1
-TB	1
-TC	1
TECHNICAL LIBRARY	
ATTN: AMSTA-AR-CCB-O	5
TECHNICAL PUBLICATIONS & EDITING SECTION	
ATTN: AMSTA-AR-CCB-O	3
OPERATIONS DIRECTORATE	
ATTN: SMCWV-ODP-P	1
DIRECTOR, PROCUREMENT & CONTRACTING DIRECTORATE	
ATTN: SMCWV-PP	1
DIRECTOR, PRODUCT ASSURANCE & TEST DIRECTORATE	
ATTN: SMCWV-QA	1

NOTE: PLEASE NOTIFY DIRECTOR, BENÉT LABORATORIES, ATTN: AMSTA-AR-CCB-O OF ADDRESS CHANGES.

TECHNICAL REPORT EXTERNAL DISTRIBUTION LIST

	NO. OF COPIES
ASST SEC OF THE ARMY RESEARCH AND DEVELOPMENT ATTN: DEPT FOR SCI AND TECH THE PENTAGON WASHINGTON, D.C. 20310-0103	1
ADMINISTRATOR DEFENSE TECHNICAL INFO CENTER ATTN: DTIC-OCP (ACQUISITION GROUP) BLDG. 5, CAMERON STATION ALEXANDRIA, VA 22304-6145	12
COMMANDER U.S. ARMY ARDEC ATTN: SMCAR-AEE	1
SMCAR-AES, BLDG. 321	1
SMCAR-AET-O, BLDG. 351N	1
SMCAR-FSA	1
SMCAR-FSM-E	1
SMCAR-FSS-D, BLDG. 94	1
SMCAR-IMI-I, (STINFO) BLDG. 59 PICATINNY ARSENAL, NJ 07806-5000	2
DIRECTOR U.S. ARMY RESEARCH LABORATORY ATTN: AMSRL-DD-T, BLDG. 305 ABERDEEN PROVING GROUND, MD 21005-5066	1
DIRECTOR U.S. ARMY RESEARCH LABORATORY ATTN: AMSRL-WT-PD (DR. B. BURNS) ABERDEEN PROVING GROUND, MD 21005-5066	1
DIRECTOR U.S. MATERIEL SYSTEMS ANALYSIS ACTV ATTN: AMXSY-MP ABERDEEN PROVING GROUND, MD 21005-5071	1
COMMANDER ROCK ISLAND ARSENAL ATTN: SMCRI-ENM ROCK ISLAND, IL 61299-5000	1
MIAC/CINDAS PURDUE UNIVERSITY P.O. BOX 2634 WEST LAFAYETTE, IN 47906	1
COMMANDER U.S. ARMY TANK-AUTMV R&D COMMAND ATTN: AMSTA-DDL (TECH LIBRARY) WARREN, MI 48397-5000	1
COMMANDER U.S. MILITARY ACADEMY ATTN: DEPARTMENT OF MECHANICS WEST POINT, NY 10966-1792	1
U.S. ARMY MISSILE COMMAND REDSTONE SCIENTIFIC INFO CENTER ATTN: DOCUMENTS SECTION, BLDG. 4484 REDSTONE ARSENAL, AL 35898-5241	2
COMMANDER U.S. ARMY FOREIGN SCI & TECH CENTER ATTN: DRXST-SD 220 7TH STREET, N.E. CHARLOTTESVILLE, VA 22901	1
COMMANDER U.S. ARMY LABCOM MATERIALS TECHNOLOGY LABORATORY ATTN: SLCMT-IML (TECH LIBRARY) WATERTOWN, MA 02172-0001	2
COMMANDER U.S. ARMY LABCOM, ISA ATTN: SLCIS-IM-TL 2800 POWER MILL ROAD ADELPHI, MD 20783-1145	1

NOTE: PLEASE NOTIFY COMMANDER, ARMAMENT RESEARCH, DEVELOPMENT, AND ENGINEERING CENTER, BENÉT LABORATORIES, CCAC, U.S. ARMY TANK-AUTOMOTIVE AND ARMAMENTS COMMAND, AMSTA-AR-CCB-O, WATERVLIET, NY 12189-4050 OF ADDRESS CHANGES.

TECHNICAL REPORT EXTERNAL DISTRIBUTION LIST (CONT'D)

	NO. OF COPIES
COMMANDER U.S. ARMY RESEARCH OFFICE ATTN: CHIEF, IPO P.O. BOX 12211 RESEARCH TRIANGLE PARK, NC 27709-2211	1
DIRECTOR U.S. NAVAL RESEARCH LABORATORY ATTN: MATERIALS SCI & TECH DIV CODE 26-27 (DOC LIBRARY) WASHINGTON, D.C. 20375	1 1
WRIGHT LABORATORY ARMAMENT DIRECTORATE ATTN: WL/MNM EGLIN AFB, FL 32542-6810	1
WRIGHT LABORATORY ARMAMENT DIRECTORATE ATTN: WL/MNMF EGLIN AFB, FL 32542-6810	1

NOTE: PLEASE NOTIFY COMMANDER, ARMAMENT RESEARCH, DEVELOPMENT, AND ENGINEERING CENTER, BENÉT LABORATORIES, CCAC, U.S. ARMY TANK-AUTOMOTIVE AND ARMAMENTS COMMAND, AMSTA-AR-CCB-O, WATERVLIET, NY 12189-4050 OF ADDRESS CHANGES.